Journal of Catalysis 325 (2015) 1–8

Contents lists available at ScienceDirect

Journal of Catalysis

journal homepage: www.elsevier.com/locate/jcat

Vapor-phase ethanol carbonylation with heteropolyacid-supported Rh

Sara Yacob [a], Sunyoung Park [a,1], Beata A. Kilos [b], David G. Barton [b], Justin M. Notestein [a,*]

[a] Northwestern University, Department of Chemical and Biological Engineering, Evanston, IL 60208, USA
[b] The Dow Chemical Company, Core R&D, Midland, MI 48674, USA

ARTICLE INFO

Article history:
Received 26 November 2014
Revised 29 January 2015
Accepted 10 February 2015

Keywords:
Carbonylation
Heteropolyacid
Ethanol
Iodide
Rhodium

ABSTRACT

Ethanol carbonylation is a potential route to valuable C3 products. Here, Rh supported on porous, Cs-exchanged heteropolyacid $Cs_3PW_{12}O_{40}$, is demonstrated as an effective catalyst for vapor-phase ethanol carbonylation, with higher selectivity and conversion to propionates than existing catalysts. Residual acidity or a Mo polyatom was strongly detrimental to yields. Propionate selectivity was maximized at 96% at 170 °C and with added H_2O. The catalyst displayed stable selectivity over 30 h on stream and up to 77% conversion. Ethyl iodide is a required co-catalyst but at levels as low as 2% relative to ethanol. XPS and *in situ* XANES indicate partial Rh reduction, consistent with the formation of low-valent reactive intermediates and slow deactivation through formation of Rh nanoparticles. With further optimization and understanding, these Rh/heteropolyacid catalysts may lead to stable and selective catalysts for the production of propionates through ethanol carbonylation.

1. Introduction

Alcohol carbonylation is an important commercialized process, particularly for the production of acetic acid from methanol, which is one of the largest industrial processes to use homogeneous catalysts [1–4]. A common system for alcohol carbonylation uses a group VIII metal complex and an iodide co-catalyst in the condensed phase. Alkyl iodides are formed *in situ*, which oxidatively add to the transition metal complex, followed by CO insertion into the M–C bond, and reductive elimination [5–7]. Much less studied are processes for the ethanol carbonylation to propionates, alcohol carbonylation in the vapor phase, or alcohol carbonylation using supported, heterogeneous catalysts. Vapor-phase heterogeneous catalysts include the mechanistically distinct carbonylation of methanol and dimethyl ether with mordenite-type zeolites [8–11], and variants on the Reppe carbonylation of ethylene [10–14]. Only a very limited number of studies have investigated solid catalysts for ethanol carbonylation to propionic acid or ethyl propionate, and all are for group VIII metals promoted with alkyl iodides [15–18]. Both Nefedov and Scurrell separately showed that Rh supported on X-type zeolites are effective heterogeneous catalysts for vapor-phase alcohol carbonylation with added iodide [15–22]. Rh has also been supported on various materials including carbon [23,24] or ligand-modified oxides [25] for carbonylation of methanol in the vapor phase. Several other insoluble resins have been developed for methanol carbonylation, both in the vapor and liquid phases. Critically, Christensen and Scurrell found decreasing selectivity for propionates with increasing ethanol conversion [15,16]. This was not due to sequential reactions, but rather due to the strong competition from ethanol dehydration to ethylene and diethyl ether. Although the references cited above demonstrate that ethylene and ethers can participate in carbonylation chemistry, the water that forms as a co-product appears to be detrimental to carbonylation reactivity in those systems. Given ethanol's strong propensity to dehydrate, this must be addressed for any acid catalyst [26,27]. Therefore, there is a need for development and testing of new catalyst formulations that suppress ethanol dehydration and promote carbonylation in the vapor phase.

An important other class of carbonylation catalysts are those based on heteropolyacids. Heteropolyacids have been widely used as homogeneous and heterogeneous acid and redox catalysts [28–30]. Limited reports have shown that these catalysts are capable of methanol [31,32] or dimethyl ether [33] carbonylation to acetic acid and methyl acetate, respectively. Both reports considered it essential to have a Brønsted acidic support. There are many structural classes of heteropolyacids such as Keggin [34], Wells–Dawson [35], Finke–Droege [36], and Pope–Jeannin–Preyssler [37]. Among the various heteropolyacids, Keggin heteropolyacids have been broadly investigated because they are the most stable and readily synthesized. Keggin heteropolyacids are comprised of heteropolyanions of the formula $[XM_{12}O_{40}]^{n-}$, where X is the

* Corresponding author. Fax: +1 847 491 3728.
E-mail address: j-notestein@northwestern.edu (J.M. Notestein).
[1] Current address: Korean Research Institute of Chemical Technology, Yueseong-gu, Deajeon 305-600, South Korea.

http://dx.doi.org/10.1016/j.jcat.2015.02.004
0021-9517/

heteroatom (P, Si, etc.) and M is the polyatom (W, Mo, etc.) [28–30,34]. Changing the heteroatom and polyatom controls the acidic and redox properties of these heteropolyacids, and these properties have been investigated in various catalytic reactions [29,30]. The use of $H_3PW_{12}O_{40}$ in alcohol and ether carbonylation has been reported [38]. Heteropolyacids are highly soluble in polar solvents including water and alcohols, while heteropolyacid salts with large cations are insoluble and have high surface area by forming a tertiary structure [28,29]. Examples of cations commonly used include K^+, Rb^+, Cs^+, and NH_4^+, and the acidity of a heteropolyacid salt can be tuned by the amount of the large cation exchanged on the heteropolyanion, leading to wide use as solid acid catalysts [28]. Cs^+-modified heteropolyacids have been demonstrated in dimethyl ether carbonylation [39].

This work describes the novel application of Rh supported on heteropolyacids as a promising heterogeneous catalyst for vapor-phase ethanol carbonylation, including identification of suitable operating conditions and catalyst compositions, spectroscopic analysis of the active catalyst, and mechanistic insight into the working state of the catalyst. The mechanism appears to be broadly analogous to that of condensed-phase methanol carbonylation by similar, soluble catalysts. As compared to existing catalysts known for vapor-phase ethanol carbonylation, the catalysts described here have higher selectivity to the desired carbonylation products, including at high conversion.

2. Experimental

2.1. Catalyst preparation

Heteropolyacid (HPA) salts were prepared through an ion-exchange method. Keggin HPAs, phosphotungstic acid $H_3PW_{12}O_{40}(H_2O)_x$, and phosphomolybdic acid $H_3PMo_{12}O_{40}(H_2O)_x$ were purchased and used as received from Sigma–Aldrich. Cs^+ or NH_4^+ was used as exchange cations. Cs^+ was incorporated with stoichiometries from $x = 1.5$–3.0 in $Cs_xH_{3-x}PW_{12}O_{40}$ or $Cs_x(NH_4)_{3-x}PW_{12}O_{40}$ to cover the range where surface area and acidity vary significantly [28]. NH_4^+ was incorporated with stoichiometries from $x = 0$–1.5 in $Cs_x(NH_4)_{3-x}PW_{12}O_{40}$. Water was purified to 18 MΩ resistivity using a Barnstead Nanopure Infinity system and passed through a 0.2 μm filter before use. A known amount of cesium nitrate ($CsNO_3$, Sigma–Aldrich) and/or ammonium nitrate (NH_4NO_3, Sigma–Aldrich) was dissolved in 20 mL of distilled water to form 0.13–0.15 M solutions and slowly added to 20 mL of 0.05 M aqueous solution of phosphotungstic acid or phosphomolybdic acid while stirring. The resulting composite solution was heated at 60 °C overnight to obtain a solid product. The solid product was dried for 1–3 h in a 150 °C oven and then calcined at 350 °C in static air for 2 h ramping at 5 °C/min.

Rh was then loaded on HPA salts by incipient wetness impregnation using $RhCl_3(H_2O)_x$ obtained from Sigma–Aldrich and used as received. Rh content was controlled in the range of 0.5–5 wt%. The impregnated solid was dried for 1–3 h in a 150 °C oven and then calcined at 350 °C in static air for 2 h ramping at 5 °C/min. A comparison Rh catalyst was synthesized on Na13X zeolite by ion exchange between $RhCl_3(H_2O)_x$ and Na13X molecular sieve (Sigma–Aldrich). The Rh precursor was dissolved in water, and a known amount of Na13X molecular sieve was added such as to make 1 wt% Rh. The resulting solution was heated to 80 °C and stirred overnight. Filtration yielded solid particles, which were washed with ~200 mL of purified water and dried in a 150 °C oven overnight. After drying, the catalyst was calcined at 400 °C in static air for 2 h ramping at 5 °C/min. These materials showed no indication of framework disruption by ^{27}Al MAS SS NMR (Appendix A, Fig. S1).

A silica-supported 1 wt% $Rh/Cs_3PW_{12}O_{40}/SiO_2$ catalyst was synthesized as follows. 1 g $H_3PW_{12}O_{40}$ was loaded onto 2 g of silica gel (Selecto Scientific, ~500 m^2/g, ~6 nm pore diameters, 40–63 μm particle size) by incipient wetness impregnation from water, dried at 150 °C for 1–3 h, and calcined at 300 °C for 2 h. 0.19 g of $CsNO_3$ was dissolved in 30 mL of distilled water. 1.9 g of $H_3PW_{12}O_{40}/SiO_2$ was then dispersed in the solution with constant stirring, and the mixture was stirred for 12 h. The solid product was filtered, washed with distilled water, dried at 150 °C for 1–3 h, and calcined at 350 °C for 2 h to obtain $Cs_3PW_{12}O_{40}/SiO_2$ support. $RhCl_3(H_2O)_x$ was then supported onto $Cs_3PW_{12}O_{40}/SiO_2$ by incipient wetness impregnation as above at a loading of 1 wt% relative to the $Cs_3PW_{12}O_{40}$. The impregnated solid was dried at 150 °C for 1–3 h and calcined at 350 °C for 2 h.

2.2. Catalyst characterization

Cs and W contents in the catalysts were determined by inductively coupled plasma-mass spectrometry (ICP-MS). Rh contents on the catalysts were measured by inductively coupled plasma-atomic emission spectrometry (ICP-AES) analysis. Materials were found to dissolve well in a solution of 95 wt% water, 3 wt% nitric acid, 1 wt% hydrofluoric acid, and 1 wt% hydrochloric acid. For calibration, samples were compared to known concentrations of Rh, Cs, and W in the same stock solutions that samples were dissolved in. All elemental ICP standard solutions were acquired from Sigma–Aldrich at an original concentration of 1000 ppm.

Surface areas of the catalysts were measured using N_2 physisorption on a Micromeritics 2010 ASAP. Prior to N_2 physisorption, all samples were degassed under vacuum overnight at 140 °C. X-ray diffraction (XRD) patterns of the catalysts were acquired using Cu Kα radiation operated at 40 kV and 20 mA using a Rigaku Geigerflex X-ray powder diffractometer. X-ray photoelectric spectroscopy (XPS) was performed on a Thermo Scientific ESCALAB 250 Xi. Peak locations were identified using Advantage Software v5.5.3. The spectrometer binding energy was calibrated through energy shifts to the reference C 1s (284.9 eV). Thermogravimetric analysis (TGA) was done on a Q500 from TA Instruments. An 80 mg sample was subjected to a temperature ramp from ambient to 350 °C at a rate of 5 °C/min under oxygen flow.

Rh K-edge X-ray absorption near edge structure (XANES) spectral measurements were performed at the Advanced Photon Source, Argonne National Laboratory. The DuPont–Northwestern–Dow Collaborative Access Team (DND-CAT) bending magnet D beamline at Sector 5 was used. XANES spectra were recorded in transmission mode by employing a Si(111) double crystal monochromator. Transmission intensities were measured with Canberra ionization chambers. For the Rh K-edge, all XANES spectra were scanned in the range of 23,100–23,450 eV. The photon energy for each scan was calibrated using Rh foil, setting the first inflection point at the known edge energy of Rh^0, 23,220 eV. 2–5 scans of each reference were averaged to optimize signal-to-noise ratio. XANES of the as-synthesized catalyst was compared to metallic Rh, Rh_2O_3, $RhCl_3(H_2O)_x$, and RhI_3.

Temperature-programmed desorption (TPD) of NH_3 was carried out in an Altamira Instruments AMI-200 to measure catalyst acidity. 0.1 g of each catalyst charged into a quartz reactor and pretreated at 200 °C for 1 h with a stream of He (25 mL/min). A mixed stream of NH_3 and He (25 mL/min) was then introduced into the reactor at 50 °C for 30 min. Physisorbed NH_3 was removed at 100 °C for 1 h under a flow of He (25 mL/min). After cooling the catalyst, furnace temperature was increased from 50 °C to 600 °C at a heating rate of 20 °C/min under a flow of He (25 mL/min). Desorbed NH_3 was detected using a thermal conductivity detector (TCD). For calibration, known amounts of NH_3 were injected into the empty reactor under a flow of He (25 mL/min).

2.3. Ethanol carbonylation flow reactor

Gas-phase reactions were carried out in quartz downflow microreactors in an Altamira Instruments BenchCAT 4000R-HP. Mixtures of ethanol and ethyl iodide co-catalyst were delivered via liquid syringe pump (KD Scientific KDS-100) at total liquid flow rates of 2–5 μL/min. The ethanol-to-ethyl iodide ratio was controlled in the range of 5–100:1. The liquid feed was vaporized in line with CO reactant. CO-to-ethanol molar ratios varied from 2 to 18:1, and CO flow rates were varied between 5 mL/min and 30 mL/min. The catalyst bed consisted of 0.1–1.5 g of catalyst held in place by quartz wool, and the reactions were conducted at reactor temperatures of 150–210 °C and nominally at atmospheric pressure. No pretreatment was performed on the catalyst bed unless otherwise stated. Weight hourly space velocities (WHSVs) were obtained from total mass flow rate divided by mass of catalyst.

Reactant and product concentrations were measured every 20 min during time on stream (TOS) using an Agilent 7890A GC-FID with helium carrier through a HP InnoWax column (50 m × 0.2 mm × 0.4 μm). The GC program included a multi-step ramp from 60 to 200 °C. Ethylene, diethyl ether (DEE), ethyl iodide (EtI), ethanol (EtOH), ethyl propionate (EP), and propionic acid (PA) eluted in that order and were the only products quantified, and they were used to report an ethyl species mass balance. CO and CO_2 are not included in this mass balance. Unless otherwise noted, this mass balance was 100 ± 10% and formally defined as: $(n_{EtOH} + n_{EtI} + n_{ethylene} + 2n_{DEE} + 2n_{EP} + n_{PA})/(n_{EtI,0} + n_{EtOH,0})$. Not able to be quantified were amounts of CO, CO_2, H_2, or H_2O due to the use of an FID detector. Conversions are reported relative to EtOH and EtI in an empty reactor and are generally ±5% over multiple trials and for a given catalyst over several hours at steady operation. Selectivity is reported relative to the total moles of products detected, as opposed to ethanol converted, and is formally given as $n_x/(n_{ethylene} + n_{DEE} + n_{EP} + n_{PA})$, where n_x refers to the molar concentrations of a given species. Unless otherwise stated, catalyst performance is given as nominally steady state values averaged over all data from 40 min to 4–5 h TOS at a given condition. In early studies, it was seen that catalyst changes were slow after 4 h.

3. Results and discussion

3.1. Catalytic performance of $Rh/(Cs,NH_4)_xH_{3-x}PM_{12}O_{40}$ (M = W, Mo)

A series of Rh-containing catalysts were prepared and compared for activity in vapor-phase EtOH carbonylation (Table 1). In this section, the ratio of CO:EtOH:EtI in the feed was fixed at 164:10:1, the WHSV was held constant at 24 h^{-1}, and the temperature was 170 °C. All reactions are at nominal 1 atmosphere total pressure.

Cs^+/H^+- and Cs^+/NH_4^+-exchanged HPAs were used as supports for 1 wt% Rh catalysts. The use of either Cs^+ or NH_4^+ during synthesis resulted in surface areas >160 m^2/g, as compared to $H_3PW_{12}O_{40}$ with a surface area <10 m^2/g. This shows that the porous, tertiary structure was developed correctly [28]. N_2 physisorption curves are shown in Appendix A Fig. S2. After calcination, the Cs^+/NH_4^+ form is chemically indistinguishable from the Cs^+/H^+ form. Regardless of whether H^+ or NH_4^+ was used during synthesis, 1 wt% Rh/Cs_x-$H_{3-x}PW_{12}O_{40}$ (x = 0, 1.5, 2.0, 2.5, 2.8, 3.0) gave EtOH conversions that decreased monotonically with increasing Cs^+ exchange at a fixed WHSV. However, for all but the fully exchanged sample, only dehydration products were synthesized with appreciable selectivity. The marked increase in EP selectivity for $Rh/Cs_3PW_{12}O_{40}$ (from 2.3% for $Cs_{2.5}$, to 5.9% for $Cs_{2.8}$, to 81.6% for Cs_3) was due to both a significant decrease in rate of dehydration and also a significant rise in the rate of EP production. The marked drop in dehydration products parallels the complete loss of acid sites for $Rh/Cs_3PW_{12}O_{40}$. The x = 2.5 and 2.8 materials still contain 38 and 25 μmol titratable H^+ sites per gram of catalyst, respectively, whereas x = 3.0 contains no significant acidity. NH_3-TPD curves for x = 2.5, 2.8, and 3 are shown in Appendix A Fig. S3. In the absence of Rh, all of these HPA salts gave only dehydration products, indicating that the Rh species is required for CO adsorption and activation [31]. For increasing Rh between 0.5 and 5 wt%, EtOH conversion slightly increased throughout the range, with EP selectivity changing little above 1 wt%. For this reason, the 1 wt% loading was the focus of all other catalytic investigations.

An important role of the polyatom was seen for 1 wt% $Rh/Cs_3PM_{12}O_{40}$ with M = W or Mo. Under standard conditions,

Table 1
EtOH carbonylation with $Rh/(Cs,NH_4)_xH_{3-x}PM_{12}O_{40}$ (M = W, Mo).[a]

Catalyst	S.A. (m^2/g)	Acidity (μmol-NH_3/g)	% Conversion		% Selectivity				Mass balance (%)
			EtOH	EtI	Ethylene	DEE	EP	PA	
1 wt% $Rh/(NH_4)_3PW_{12}O_{40}$	201		87.7	4.8	83.7	10.6	4.2	1.5	112.5
1 wt% $Rh/Cs_{1.5}(NH_4)_{1.5}PW_{12}O_{40}$	189		90.0	6.9	84.1	9.5	4.5	2.0	111.4
1 wt% $Rh/Cs_2(NH_4)_1PW_{12}O_{40}$	170		88.2	4.6	86.3	9.3	3.3	1.1	108.3
1 wt% $Rh/Cs_{2.5}(NH_4)_{0.5}PW_{12}O_{40}$	165		66.3	7.0	43.5	52.3	3.0	1.2	89.8
1 wt% $Rh/Cs_{2.5}H_{0.5}PW_{12}O_{40}$	159	37.7	52.6	2.7	39.5	57.9	2.3	0.4	93.9
1 wt% $Rh/Cs_{2.8}H_{0.2}PW_{12}O_{40}$	159	25.4	38.0	<1	24.8	69.3	5.9	0	92.1
1 wt% $Rh/Cs_3PW_{12}O_{40}$	162	Trace	8.7	6.1	11.4	7.0	81.6	0	95.3
$Cs_{2.5}H_{0.5}PW_{12}O_{40}$			64.0	3.0	43.6	56.4	0	0	93.7
$Cs_{2.8}H_{0.2}PW_{12}O_{40}$			52.0	<1	13.4	86.6	0	0	99.3
$Cs_3PW_{12}O_{40}$			<1	<1	17.9	82.1	0	0	102.4
0.5 wt% $Rh/Cs_3PW_{12}O_{40}$			6.8	8.4	22.8	4.8	72.5	0	95.9
1 wt% $Rh/Cs_3PW_{12}O_{40}$			8.7	6.1	11.4	7.0	81.6	0	95.3
3 wt% $Rh/Cs_3PW_{12}O_{40}$			11.0	11.1	9.8	10.2	80.0	0	93.5
5 wt% $Rh/Cs_3PW_{12}O_{40}$			11.3	7.4	11.4	10.1	78.4	0	92.8
1 wt% $Rh/Cs_3PMo_{12}O_{40}$			1.9	<1	26.4	7.4	20.5	45.7	99.0
1 wt% $Rh/Cs_3PMo_{12}O_{40}$[b]			2.3	2.8	28.7	12.1	29.4	29.9	98.0
1 wt% $Rh/Cs_3PW_{12}O_{40}/SiO_2$			23.4	<1	14.2	81.5	2.9	1.3	93.5
1 wt% Rh/Na13X	890	850	12.3	9.9	59.9	28.4	11.7	0	94.2

[a] Reaction conditions: CO:EtOH:EtI = 164:10:1, WHSV = 24 h^{-1}, 170 °C, average of 5 h TOS.
[b] WHSV = 1.6 h^{-1}, average of 7 h TOS, otherwise same conditions.

EtOH conversion was very low over $Rh/Cs_3PMo_{12}O_{40}$ and propionate selectivities were somewhat lower than for $Rh/Cs_3PW_{12}O_{40}$. At lower space velocities, neither conversions nor PA selectivities improved, and the catalyst became dark blue after 7 h on stream, indicating reduction of the phosphomolybdic acid. It has been reported that acidic and redox properties of HPAs can be controlled by changing polyatom [29,30]. Since both catalysts had all acidity titrated away, the electronic/redox properties of the W-containing HPA anion itself are specific for increasing stability, activity, and selectivity in EtOH carbonylation.

One material was prepared consisting of $H_3PW_{12}O_{40}$, Cs^+, and Rh^{3+} sequentially deposited on silica gel. EtOH conversion over $Rh/Cs_3PW_{12}O_{40}/SiO_2$ was higher than that over unsupported $Rh/Cs_3PW_{12}O_{40}$, while EP selectivity was much lower than that over unsupported $Rh/Cs_3PW_{12}O_{40}$. Even though the composition of this catalyst is in the same ratios as for the unsupported HPA salts, use of the silica support may lead to incomplete exchange of Cs^+ for acid sites and poor contact between Rh and the HPA salt, which would both be detrimental to propionate selectivity.

Finally, Table 1 also includes a benchmark 1 wt% Rh/Na13X catalyst, known for EtOH carbonylation [15–18]. The Rh/Na13X gave EtOH conversions and propionate selectivity comparable to published work (e.g. 12% selectivity) and markedly inferior to the results disclosed here [18]. Selectivity patterns of this reference catalyst appear to be weakly impacted by calcination conditions (Appendix A, Table S1).

3.2. Effect of temperature and feed composition

A 1 wt% $Rh/Cs_3PW_{12}O_{40}$ catalyst was used to investigate the dependence of temperature and other process conditions. Standard conditions were 1 atm nominal total pressure, 170 °C, 24 h^{-1}, 5 h time on stream, and a feed ratio of CO:EtOH:EtI = 164:10:1. A single parameter was varied at a time. First, the temperature was controlled between 150 and 210 °C increasing in 20 °C increments, and the results are shown in Fig. 1. EtOH conversion increased with increasing reaction temperature up to 190 °C. Ethylene selectivity increased monotonically, while DEE selectivity decreased. Carbonylation selectivity (EP + PA) passed through a clear maximum at 170 °C. PA was only detectable at 210 °C, presumably a consequence of the high water partial pressure in the reactor outlet arising from the high conversion to ethylene and attendant release of water.

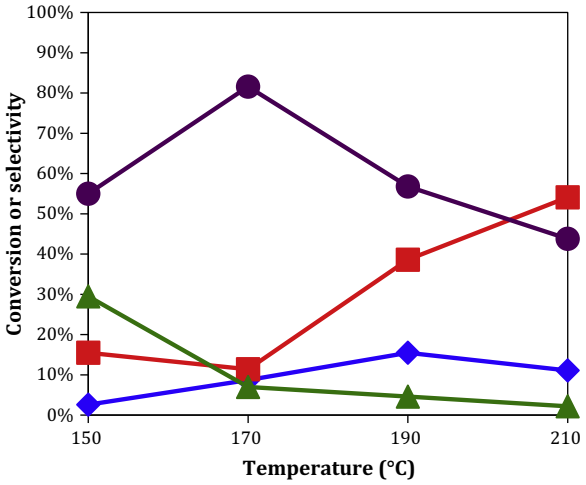

Fig. 1. EtOH carbonylation with 1 wt% $Rh/Cs_3PW_{12}O_{40}$ at various temperatures and differential conversion. Reaction conditions: CO:EtOH:EtI = 164:10:1, WHSV = 24 h^{-1}, average of 5 h TOS. Ethyl species mass balance 95 ± 5%. ♦ EtOH conversion, ■ ethylene selectivity, ▲ DEE selectivity, and ● EP + PA selectivity.

Second, the dependence of CO partial pressure was examined at 1 atm and below, and at standard conditions, the results are shown in Table 2. N_2 replaced CO to maintain constant WHSV. EtOH conversion is essentially independent of CO partial pressure over this range, consistent with the rate limiting step over Rh-iodides being the oxidative addition of the ethyl species [5,7,15,16]. EP selectivity begins to decrease for partial pressures below 0.6 atm, indicating a nearly CO-saturated catalyst under typical conditions. Similar dependences have been seen for molecular catalysts in solution, consistent with the elimination of most of the parallel, acid-catalyzed reactivity of the support [1,2,4].

Table 3 shows the effect of EtOH:EtI molar feed ratio for values between 5:1 and 100:1, as well as for pure EtI and EtOH liquid feeds, at otherwise standard conditions and constant total liquid flow rates. With only EtOH or EtI, the catalyst was essentially inert, with neither carbonylation nor dehydration products observed. Without the iodide co-catalyst, the ethyl species is assumed to be unable to enter the Rh catalytic cycle. The lack of products in the EtOH-free case indicates that the acyl iodide of classical Rh mechanisms does not appear to be able to exit from the catalytic cycle, or it indicates that the catalyst rapidly deactivates under these high halogen feed conditions. The moderately acidic $Rh/Cs_{2.5}H_{0.5}PW_{12}O_{40}$ catalyst is similarly unreactive with EtI and results only in dehydration products for EtOH-only feeds. With the mixtures of both EtOH and EtI, neither EtOH conversion nor EP selectivity changed substantially until the EtOH:EtI ratio

Table 3
EtOH carbonylation with 1 wt% $Rh/Cs_3PW_{12}O_{40}$ and various EtOH:EtI feed ratios.[a]

EtOH:EtI molar ratio	EtOH conv. (%)	EtI conv. (%)	Ethylene sel. (%)	DEE sel. (%)	EP sel. (%)	PA sel. (%)	Mass balance (%)
EtI[b]	–	5.8	100	0	0	0	102.5
EtI	–	<1	0	0	0	0	104.6
5:1	8.7	4.6	13.0	7.8	79.2	0	96.7
10:1	8.7	6.1	11.4	7.0	81.6	0	95.3
20:1	8.1	7.0	9.6	7.6	82.8	0	95.3
50:1	8.2	3.4	10.4	8.3	81.4	0	93.7
100:1	5.6	2.5	9.6	10.2	80.2	0	95.6
EtOH	1.4	–	0	0	0	0	98.6
EtOH[b]	67.3	–	40.8	59.2	0	0	93.9

[a] Reaction conditions: WHSV = 24 h^{-1}, 170 °C, average of 5 h TOS.
[b] With 1 wt% $Rh/Cs_{2.5}H_{0.5}PW_{12}O_{40}$.

Table 2
EtOH carbonylation with 1 wt% $Rh/Cs_3PW_{12}O_{40}$ at various CO partial pressures.[a]

CO partial pressure	CO:EtOH molar ratio	EtOH conv. (%)	EtI conv. (%)	Ethylene sel. (%)	DEE sel. (%)	EP sel. (%)	PA sel. (%)	Mass balance (%)
0.92[b]	16.4:1	8.7	6.1	11.4	7.0	81.6	0	95.3
0.61	10.9:1	9.4	5.4	13.9	3.4	82.7	0	95.0
0.46	8.2:1	9.2	5.2	23.4	3.9	72.3	0	95.3
0.31	5.5:1	7.6	6.5	34.6	4.7	60.7	0	95.6
0.15	2.7:1	9.9	3.0	70.7	4.8	24.5	0	92.6

[a] Reaction conditions: EtOH:EtI = 10:1, WHSV = 24 h^{-1}, 170 °C, average of 5 h TOS.
[b] At these conditions, CO conversion is approximately 0.5% estimated from detected carbonylation products.

Table 4
EtOH carbonylation with 1 wt% $Rh/Cs_3PW_{12}O_{40}$ and added H_2O.[a]

CO:H_2O:EtOH:EtI molar ratio	EtOH conv. (%)	EtI conv. (%)	Ethylene sel. (%)	DEE sel. (%)	EP sel. (%)	PA sel. (%)	Mass balance (%)
164:0:10:1	8.7	6.1	11.4	7.0	81.6	0	95.3
164:19:10:1	8.6	6.9	7.5	10.3	77.6	4.6	93.3
164:37:10:1	5.0	6.5	4.3	4.8	32.8	58.2	97.7
164:56:10:1	3.4	2.5	1.6	1.8	10.4	86.2	105.1
60:9:0:1[b]	–	25.0	4.3	0.4	0.3	72.2	87.8

[a] Reaction conditions: WHSV = 24 h^{-1}, 170 °C, average of 5 h TOS.
[b] Not shown in the table is 22.9% selectivity toward EtOH.

Table 5
EtOH carbonylation with 1 wt% $Rh/Cs_3PW_{12}O_{40}$ under various WHSV.[a]

WHSV (h^{-1})	Conversion %		Selectivity %				Mass balance (%)
	EtOH	EtI	Ethylene	DEE	EP	PA	
24	8.7	6.1	11.4	7.0	81.6	0	95.3
16	10.7	5.4	14.9	5.7	79.4	0	95.4
3.2	33.9	5.5	17.9	6.8	75.3	0	88.0
1.6	59.9	4.4	12.6	8.1	79.3	0	79.9
1.1	77.2	1.2	14.4	4.8	80.8	0	72.6

[a] Reaction conditions: CO:EtOH:EtI = 164:10:1, 170 °C, average of 5 h TOS.

exceeded 50:1. This catalyst is able to produce EP selectively at lower levels of iodide than previously reported catalysts for EtOH carbonylation [15].

Finally, 1 wt% $Rh/Cs_3PW_{12}O_{40}$ was used to determine the effect of H_2O concentration on EtOH carbonylation at standard conditions as shown in Table 4. The CO:EtOH:EtI feed ratio was fixed at 164:10:1. H_2O was added as a second liquid feed at in the feed ratio range of 0 – 56:10 for H_2O:EtOH. Selectivity to dehydration products decreased with increasing H_2O feed, consistent with these reactions being reversible. Ethylene and DEE were almost suppressed completely at the highest H_2O feed rates, and without the competitive dehydration, the selectivity to EP and PA increased to ~97%. Within the propionates, PA was increasingly favored with increasing H_2O feed rates. Conversion appears to decrease with increasing H_2O feed, although the changes may be within available precision at these WHSV. Additionally, during a test when no EtOH was included (CO:H_2O:EtOH:EtI = 60:9:0:1), virtually all propionate selectivities went to PA, as shown in the last entry of Table 4.

3.3. Effect of weight hourly space velocity (WHSV) and time on stream

The results show high propionate selectivity at low conversions typical of high space velocities. Prior work has shown decreasing propionate selectivity with increasing conversion [15,16], and the same conclusion would be drawn using only the data in Table 1. Instead, in Table 5, WHSV was controlled between 1.1 and 24 h^{-1} with 1 wt% $Rh/Cs_3PW_{12}O_{40}$ at 170 °C and 1 atm for 5 h TOS with a CO:EtOH:EtI feed ratio of 164:10:1. As expected, EtOH conversion increased significantly with decreasing WHSV, but EP selectivity was remarkably constant at all space velocities tested. It should be noted that even for the highest conversions in Table 5, reactive ethyl (EtOH + EtI) concentrations in the effluent are comparable to those of H_2O. Thus, substantial excess H_2O, such as in Table 4, is required to see any significant EP hydrolysis to PA for this system. These results are consistent with dehydration and carbonylation being parallel pathways. We must note, however, that at the lowest space velocities, ethyl species mass balances are poor, indicating the formation of undetectable products. Although individual runs show poor mass balance at low WHSV, conversions and selectivities were reproducible to within 5% and 3% error, respectively, over multiple catalyst preparations and catalytic runs, showing that the reaction is not intrinsically unstable. Explicit batch-to-batch variability is shown in Appendix A Table S2.

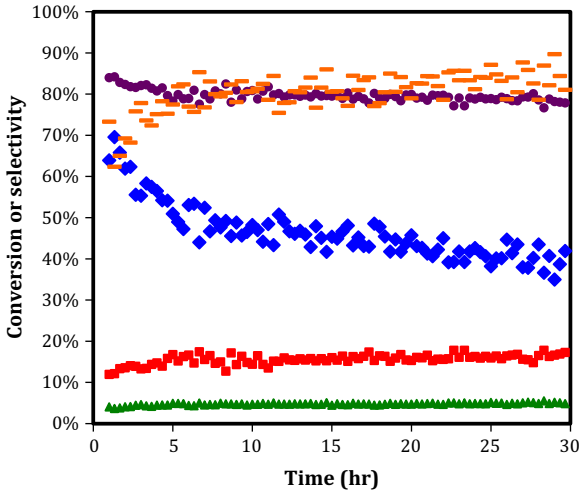

Fig. 2. Catalytic performance with time on stream in EtOH carbonylation over 1 wt% $Rh/Cs_3PW_{12}O_{40}$ for 30 h. WHSV = 1.6 h^{-1}, 1 atm nominal total pressure, 170 °C, feed ratio of CO:EtOH:EtI = 164:10:1. ♦ EtOH conversion, ■ ethylene selectivity, ▲ DEE selectivity, and ● EP + PA selectivity, – mass balance.

An extended reaction of 30 h TOS was carried out at a WHSV of 1.6 h^{-1} and standard conditions as shown in Fig. 2. EtOH conversion decreased from ~65% to ~50% over the first 6 h, but decayed much slower over the subsequent 24 h. EP selectivity remained nearly constant at ~80% for the entire run. The mass balance improved progressively throughout the run, eventually stabilizing out at ~85%.

A sample of catalyst recovered after a similar experiment at 10 h on stream lost 3.7 wt% during subsequent TGA in O_2 up to 350 °C, the typical initial calcination temperature. This mass loss corresponds to approximately 1.6 mmol carbon per 50 mg catalyst or approximately 3% of the EtOH feed over the 10 h run. Thus, only a fraction of the incomplete mass balance can be accounted for by deposition of easily removed carbon. Presumably, the remaining unaccounted species are heavier species trapped elsewhere in the reactor system or species undetected by the current GC method. Given the large amounts of HI generated in the reactor at low WHSV, rearrangement to heavier, undetected products such as ethylene oligomers is not unexpected, and a gradual baseline

rise is noticed in the GC traces of these experiments. All thermal treatments intended to regenerate the catalyst were ultimately detrimental to performance, but none altered the crystal structure of the HPA (Appendix A Table S3 and Fig. S4), suggesting that formation of Rh(0) nanoparticles and subsequent aggregation is one possible origin of deactivation, which will be discussed further below [40,41]. Increasing conversion with decreasing WHSV is expected to generate H_2 from residual water gas shift activity of the Rh catalyst [42], which could exacerbate this process.

3.4. Spectroscopic analysis

In situ XANES was used to examine the oxidation state of the catalyst during reaction conditions. A least-squares linear combination fit was conducted using known reference standards: metallic Rh, Rh_2O_3, $RhCl_3$, and RhI_3 (Figs. S5 and S6a). The fresh 5 wt% Rh/$Cs_3PW_{12}O_{40}$ catalyst was well fit as a combination of Rh_2O_3 (21%) and $RhCl_3$ (79%) character, both trivalent Rh species. This fit implies the freshly prepared catalyst contains Rh(III) species in a mixture of Cl and O coordination. Good agreement could not be reached when excluding $RhCl_3$ standard from the least-squares linear combination fit. As anticipated, the fresh catalyst contains no metallic Rh or RhI_3 character.

The catalyst was examined with XANES during standard reaction conditions using an *in situ* cell, Fig. 3. Spectra were fit every hour as a combination of the standards. In this manner, the Rh_2O_3 and $RhCl_3$ species content decreased significantly, beginning immediately after the *in situ* reaction began. Likewise, principal component analyses revealed RhI_3 character shortly after the *in situ* reaction began, indicating the formation of metal–iodide bonds when feeding EtI (Appendix A Fig. S7). Also, evident via the principal component analysis is the decrease in the average oxidation state during the first two hours. After two hours on stream, the catalyst did not show any additional significant changes. The used catalyst after 10 h on stream was fit to a mixture of Rh, RhI_3, and $RhCl_3$, corresponding to an average oxidation state of ~1.8 (Appendix A Fig. S6b). Fits of the used catalyst excluding metallic Rh or RhI_3 standards were both found inadequate. This decrease in average oxidation state is consistent both with slow activation of the catalyst to form Rh(I) reactive intermediates analogous to solution-phase catalysts and the possible formation of Rh(0) nanoparticles as a deactivation route.

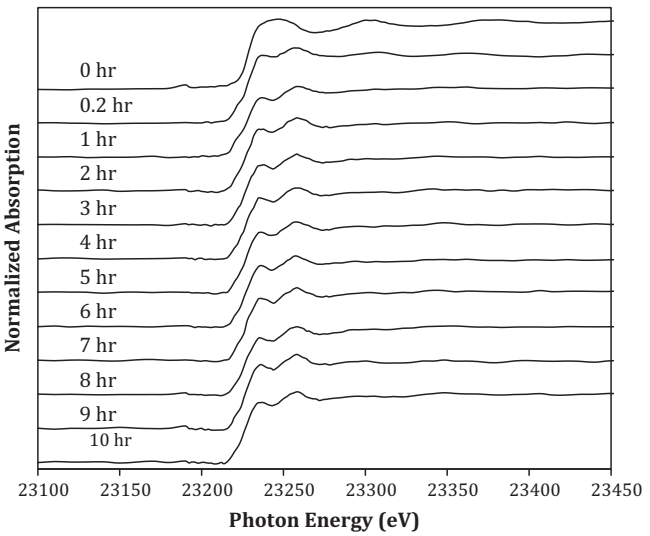

Fig. 3. *In situ* XANES spectra over 5 wt% Rh/$Cs_3PW_{12}O_{40}$ for 10 h. WHSV ~ 24 h^{-1}, 1 atm nominal total pressure, 170 °C, feed ratio of CO:EtOH:EtI = 164:10:1.

Table 6
Rh $3d_{5/2}$ binding energies for Rh/$Cs_3PW_{12}O_{40}$ before and after various treatments.

Catalyst and treatment	Rh $3d_{5/2}$ binding energy (eV)
Rh/$Cs_3PW_{12}O_{40}$ fresh	308.3
Rh/$Cs_3PW_{12}O_{40}$ used	307.0
Rh/$Cs_3PW_{12}O_{40}$ fresh, reduced at 400 °C	306.5
Rh/$Cs_3PW_{12}O_{40}$ regenerated	307.9
Rh_2O_3 [43,44]	308.5
Rh foil [45]	307.2
Supported Rh^0 nanoparticles [46]	306.8

Samples of the fresh and used catalysts were also examined using XPS to support the changes in the average Rh oxidation state seen from *in situ* XANES. Table 6 shows Rh $3d_{5/2}$ binding energies (±0.5 eV due to low Rh loadings), and XPS scans are collected in Appendix A Fig. S8. The fresh catalyst has a Rh $3d_{5/2}$ binding energy of 308.3 eV, within uncertainty of the literature assignment of Rh(III) oxide at 308.5 eV [43,44]. After the catalyst has been used at standard conditions and re-exposed to air during sample transfer, the binding energy decreased to 307.0 eV. Analysis of a fresh catalyst deliberately reduced in H_2 at 400 °C for 2 h gave a similar binding energy of 306.5 eV. Both measurements are within error of typical binding energies of the bulk metal, 307.2 eV [45] and of reported values for supported Rh nanoparticles, 306.8 eV [46]. An attempt was made to regenerate the used catalyst by calcination at 350 °C in static air for 2 h. The regenerated catalyst was only partially re-oxidized with a binding energy of 307.9 eV. Overall, the XPS results are consistent with partial reduction of the catalyst during reaction witnessed via *in situ* XANES. Specifically, XPS suggests that the catalyst contained significant Rh(0) content and that these Rh(0) nanoparticles could not be re-oxidized under typical calcination conditions. This further supports the hypothesis that reduction to Rh(0) nanoparticles may be the root cause for deactivation in these materials.

3.5. Isotopic labeling study

EtOH carbonylation was also carried out with isotopically labeled reagents to help understand the reaction network. 99% of the feed EtI was labeled at the primary carbon, $^{13}EtI = CH_3{}^{13}CH_2I$. Standard reaction conditions were used consisting of 1 atm nominal pressure, CO:EtOH:^{13}EtI of 164:10:1, WHSV of 24 h^{-1}, and temperature of 170 °C using the reference 1 wt% Rh/$Cs_3PW_{12}O_{40}$ catalyst. Products are analyzed by an Agilent 5975C GC–MS after 2 h TOS. Under these conditions, the exiting organic liquids are approximately 8.5% EtI, 83% EtOH, 1% ethylene, 0.5% DEE, and 7% EP. Mass spectra fragmentation patterns are collected in Appendix A Fig. S9.

The mass spectrum for EtI peak showed a mixture of ^{12}C (38%) and ^{13}C (62%) EtI; the appearance of unlabeled ^{12}C EtI indicates that EtI is formed from the ^{12}C EtOH. Further, ^{13}C is incorporated into the propionate fragment of EP at nearly the same level of isotope incorporation (^{12}C 35% and ^{13}C 65%), consistent with a mechanism where the EtI adds to the Rh center, eventually leading to formation of an acyl group. ^{13}C is found in DEE (^{12}C 66%, ^{13}C 31%, ^{13}C double incorporation 2%), indicating the reaction of ^{13}EtI and EtOH. No significant label is seen in EtOH or in the ethoxy fragment of EP. Preferred condensation reactions with EtI are therefore consistent with the much higher concentration of EtOH (83%) than propionate groups (7%) or water (1–2% by stoichiometry).

Considering the results presented here, we propose the mechanism for EtOH carbonylation over Rh/$Cs_3PW_{12}O_{40}$ catalyst to be analogous to established mechanisms for methanol carbonylation shown in Fig. 4 [5–7]. In this analogous mechanism, a Rh–ethyl complex is formed by addition of EtI to a Rh(I) anion. The

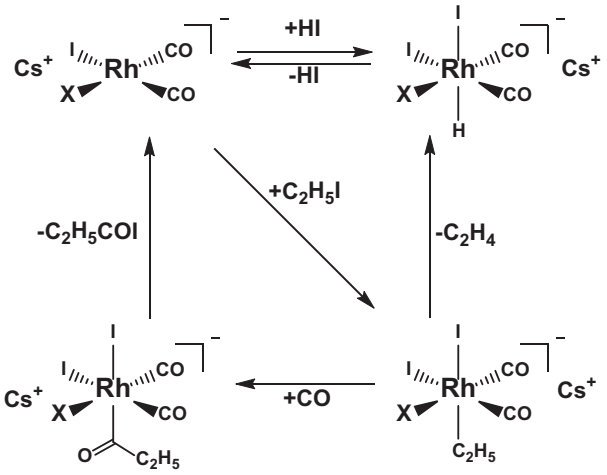

Fig. 4. Proposed mechanism for EtOH carbonylation. In addition, acid-catalyzed, reversible reactions interconnect acyl iodide to PA and EP via reaction with HI, H_2O, or EtOH. A similar network exists for the interconversion of EtI, EtOH, DEE, and ethylene. The X ligand may be HPA, iodide, or some other species, with the exact nature of the coordination not known at this time.

resulting Rh(III) species can either undergo migratory insertion of CO into the Rh–ethyl bond, as is typical, or β-hydride elimination to produce ethylene, and eventually HI and the starting Rh(I) complex. The latter steps would not be found in the methanol mechanism but are possible here. The Rh–acyl complex then eliminates the acyl iodide to complete the catalytic cycle. In steps not likely catalyzed by the Rh center, the acyl iodide is condensed with EtOH (or water in certain cases) and HI reacts with EtOH to regenerate EtI. In side reactions that are likely close to equilibrium, EtOH and/or EtI can form DEE or ethylene, and PA can condense with EtOH or EtI. In addition, large amounts of gas-phase HI, as found at the lower space velocities, would lead to a number of acid-catalyzed side reactions, such as the formation of oligomers and rearrangement side products, not necessarily all detected, and contribute to the poor ethyl species mass balance at low WHSV.

The exact role of the HPA salt remains less clear. Its most important features are that it is a redox-stable, porous support, free of acidity. Most direct roles of the HPA acid sites can be ruled out, as even small amounts of acidity result almost exclusively in ethanol dehydration. Given that alkali iodide salts such as CsI stabilize and promote Rh carbonylation catalysts [47], the HPA salt may simply be a particularly effective source of Cs. Direct coordination of the polyatom to an active Rh(I) complex also cannot be ruled out. In either case, the possible structures, and thus mechanisms, are quite analogous to those of homogenous methanol carbonylation.

4. Conclusion

This study has demonstrated that the requirements for a high yielding, vapor-phase EtOH carbonylation catalyst are negligible acidity coming from >95% exchange of the protons in the HPA support with alkali, a W polyatom, and Rh. Other known catalysts for ethanol carbonylation in the gas phase, such as Rh/Na13X, are markedly slower and less selective, and those same supported Rh catalysts for *methanol* carbonylation report rates only approximately threefold that of the ethanol carbonylation rates reported here [15], making ethanol carbonylation a competitive process. Sequentially impregnating all catalyst components on an inert SiO_2 support was strongly detrimental to selectivity, indicating that intimate mixing of Rh, Cs, and the HPA anion is required. Spectroscopic studies using *in situ* XANES reveal Cl and O coordination in the fresh catalyst and immediate gains in I coordination after the reaction begins. XPS and XANES also show that changes in coordination during reaction are coupled with an overall drop in average oxidation state consistent with a presumed Rh(I) active state. Dependencies on reactants and isotopic incorporation indicate that the mechanism is Rh-centered and includes the oxidative addition of an alkyl iodide co-catalyst to the metal. Overall, the evidence presented above suggests that the HPA anion is primarily a stable support with no detrimental redox chemistry little direct role as an acid catalyst. Thus, other soft cations and large, weakly coordinating counter-anions may therefore be alternate methods for supporting an active catalyst.

Regarding process conditions, these catalysts give remarkably stable selectivity to propionates (80–85%) when all acidity is removed. Selectivity is unchanged at up to ~75% EtOH conversion holding all other standard conditions constant apart from WHSV. Selectivity to propionates increases further to ~95% with added water, and PA is the overwhelming product, at the expense of some conversion. EtI feed can be reduced at least fivefold relative to standard feed compositions of 10:1 EtOH:EtI with no detrimental reactivity effects. At low space velocities, ethyl species mass balances begin to suffer, indicating generation of undetectable carbon-containing species. Similarly, these catalysts deactivate slowly and have worse mass balances at low WHSV. The exact cause of deactivation and loss of mass balance is not clear at this time, but neither appears to be related to extensive coking. There is some spectroscopic evidence from changes to the Rh average oxidation state that deactivation may be caused by reduction of the Rh to metallic nanoparticles. Additional experiments are underway to use X-ray absorption spectroscopy, FTIR, and other tools to understand catalyst speciation under process conditions. Further optimizing catalyst precursors, calcination temperatures and other synthesis parameters may improve activity by placing more of the Rh in an active form. Likewise, process optimization of EtI and water feed rates, WHSV, and other operating parameters may further stabilize this catalytic system for the selective conversion of ethanol to valuable propionate oxygenates.

Acknowledgments

This work was supported by The Dow Chemical Company. Portions of this work were performed at the DuPont–Northwestern–Dow Collaborative Access Team (DND-CAT) located at Sector 5 of the Advanced Photon Source (APS). DND-CAT is supported by E.I. DuPont de Nemours & Co., The Dow Chemical Company and Northwestern University. Use of the APS, an Office of Science User Facility operated for the U.S. Department of Energy (DOE) Office of Science by Argonne National Laboratory, was supported by the U.S. DOE under Contract No. DE-AC02-06CH11357. The authors highly appreciate Dr. Qing Ma at DND-CAT of APS for his X-ray absorption spectroscopy expertise. Metal analysis (ICP-MS) was performed at the Northwestern University Quantitative Bioelemental Imaging Center generously supported by NASA Ames Research Center NNA06CB93G. Metal analysis (ICP-AES) and Solid State NMR were performed at the Northwestern University Integrated Molecular Structure Education and Research Center with funding provided by NSF DMR-0521267. The CleanCat Core facility acknowledges funding from the Department of Energy (DE-FG02-03ER15457) used for the purchase of the Altamira AMI-200. This work made use of the J.B. Cohen X-Ray Diffraction Facility supported by the MRSEC program of the National Science Foundation (DMR-1121262) at the Materials Research Center of Northwestern University. This XPS work was performed in the Keck-II facility of NU*ANCE* Center at Northwestern University. The NU*ANCE* Center is supported by NSEC (NSF EEC-0647560), MRSEC (NSF DMR-1121262), the Keck Foundation, the State of Illinois, and Northwestern University.

Appendix A. Supplementary material

Supplementary data associated with this article can be found, in the online version, at http://dx.doi.org/10.1016/j.jcat.2015.02.004.

References

[1] J.F. Roth, J.H. Craddock, A. Hershman, F.E. Paulik, Chem. Technol. 1 (1971) 600.
[2] F.E. Paulik, J.F. Roth, Chem. Commun. (1968) 1578.
[3] D.J. Forster, J. Chem. Soc. 98 (1976) 846.
[4] P.M. Maitlis, A. Haynes, G.J. Sunley, M.J. Howard, J. Chem. Soc. Dalton Trans. (1996) 2187.
[5] T.W. Dekleva, D. Forster, J. Am. Chem. Soc. 107 (1985) 3565.
[6] T.W. Dekleva, D. Forster, J. Mol. Catal. 33 (1985) 269.
[7] D. Forster, T.W. Dekleva, J. Chem. Educ. 63 (1986) 204.
[8] P. Cheung, A. Bhan, G.J. Sunley, E. Iglesia, Angew. Chem. Int. Ed. 45 (2006) 1617.
[9] E. Iglesia, J.G. Sunley, D.J. Law, A. Bhan, To the Regents of the University of California, BP Chemicals Ltd., US Patent 7 507 855, 2009.
[10] G. Kiss, Chem. Rev. 101 (2001) 3435.
[11] C.W. Bird, Chem. Rev. 62 (1962) 283.
[12] W.F. Gresham, R.E. Brooks, To Du Pont, US Patent 2 448 368, 1948.
[13] W. Reppe, H. Kröper, German Patent 863 194, 1953.
[14] W. Reppe, H. Kröper, Justus Liebigs Ann. Chem. 582 (1953) 38.
[15] B. Christensen, M.S. Scurrell, J. Chem. Soc. Faraday Trans. I 73 (1977) 2036.
[16] B. Christensen, M.S. Scurrell, J. Chem. Soc. Faraday Trans. I 74 (1978) 2313.
[17] M.S. Scurrell, T. Hauberg, Appl. Catal. 2 (1982) 225.
[18] B.K. Nefedov, R.V. Dzhaparidze, O.G. Mamaev, Bull. Acad. Sci. USSR Div. Chem. Sci. 27 (1978) 1448.
[19] S.L.T. Andersson, M.S. Scurrell, J. Catal. 71 (1981) 233.
[20] S.L.T. Andersson, M.S. Scurrell, J. Catal. 59 (1979) 340.
[21] B.K. Nefedov, R.V. Dzhaparidze, Y.T. Eidus, Bull. Acad. Sci. USSR Div. Chem. Sci. 26 (1977) 1310.
[22] B.K. Nefedov, R.V. Dzhaparidze, O.G. Mamaev, N.S. Sergeeva, Bull. Acad. Sci. USSR Div. Chem. Sci. 28 (1979) 348.
[23] R.G. Schultz, US Patent 3 689 553, 1972.
[24] R.G. Schultz, P.D. Montgomery, J. Catal. 13 (1969) 105.
[25] J. Evans, S.L. Scruton, To BP Chemicals Limited, The University of Southampton, US Patent 5 185 462, 1993.
[26] J.F. DeWilde, H. Chiang, D.A. Hickman, C.R. Ho, A. Bhan, ACS Catal. 3 (2013) 798.
[27] H. Chiang, A. Bhan, J. Catal. 271 (2010) 251.
[28] T. Okuhara, N. Mizuno, M. Misono, in: D.D. Eley, W.O. Haag, B. Gates (Eds.), Advances in Catalysis, vol. 41, Elsevier Academic Press Inc., San Diego, 1996, p. 113.
[29] I.V. Kozhevnikov, Chem. Rev. 98 (1998) 171.
[30] B.S. Jaynes, C.L. Hill, J. Am. Chem. Soc. 117 (1995) 4704.
[31] L.D. Dingwall, A.F. Lee, J.M. Lynam, K. Wilson, L. Olivi, J.M.S. Deeley, S. Gaemers, G.J. Sunley, ACS Catal. 2 (2012) 1368.
[32] R.W. Wegman, A.G. Abatjoglou, A.M. Harrison, J. Chem. Soc. Chem. Commun. 24 (1987) 1981.
[33] M.V. Luzgin, M.S. Kazantsev, G.G. Volkova, W. Wang, A.G. Stephanov, J. Catal. (2010) 72.
[34] J.F. Keggin, Nature 131 (1933) 908.
[35] B. Dawson, Acta Crystallogr. 6 (1953) 113.
[36] R.G. Finke, M.W. Droege, Inorg. Chem. 22 (1983) 1006.
[37] M.H. Alizadeh, S.P. Harmalker, Y. Jeannin, J. Martinfrere, M.T. Pope, J. Am. Chem. Soc. 107 (1985) 2662.
[38] R.W. Wegman, US Patent 5 218 140, To Union Carbide Chemicals & Plastics Technology Corporation, 1988.
[39] G.G. Volkova, L.M. Plyasova, A.N. Salanov, G.N. Kustova, T.M. Yurieva, V.A. Likholobov, Catal. Lett. 80 (2002) 175.
[40] K. Paredis, L.K. Ono, F. Behafarid, Z.F. Zhang, J.C. Yang, A.I. Frenkel, B.R. Cuenya, J. Am. Chem. Soc. 133 (2011) 13455.
[41] D.H. Mei, R. Rousseau, S.M. Kathmann, V.A. Glezakou, M.H. Engelhard, W.L. Jiang, C.M. Wang, M.A. Gerber, J.F. White, D.J. Stevens, J. Catal. 271 (2010) 325.
[42] E. Trabuco, P.C. Ford, J. Mol. Catal. A – Chem. 148 (1999) 1.
[43] Y. Okamoto, N. Ishida, T. Imanaka, S. Teranishi, J. Catal. 58 (1979) 82.
[44] V.I. Nefedov, M.N. Firsov, I.S. Shaplygin, J. Electron Spectrosc. 26 (1982) 65.
[45] M. Cardona, L. Ley, Photoemission in Solids I. General Principles, vol. 26, Springer, Berlin Heidelberg, 1978.
[46] A. Berko, I. Ulrych, K.C. Prince, J. Phys. Chem. B 102 (1998) 3379.
[47] B.L. Smith, G.P. Torrence, M.A. Murphy, A. Aguilo, J. Mol. Catal. 39 (1987) 115.